

# Nanostructured Silica Materials As Drug-Delivery Systems for Doxorubicin: Single Molecule and Cellular Studies

Timo Lebold, Christophe Jung, Jens Michaelis, and Christoph Bräuchle\*

*Department of Chemistry and Biochemistry, Center for Nanoscience (CeNS) and Center for Integrated Protein Science Munich (CIPSM), Ludwig-Maximilians-Universität München, Butenandtstrasse 11, Gerhard-Ertl-Building, 81377 Munich, Germany*

Received April 7, 2009; Revised Manuscript Received June 16, 2009

## ABSTRACT

We apply mesoporous thin silica films with nanometer-sized pores as drug carriers and incorporate the widely used anticancer drug Doxorubicin. Through single-molecule based measurements, we gain mechanistic insights into the drug diffusion inside the mesoporous film, which governs the drug-delivery at the target-site. Drug dynamics inside the nanopores is controlled by pore size and surface modification. The release kinetics is determined and live-cell measurements prove the applicability of the system for drug-delivery. This study demonstrates that mesoporous silica nanomaterials can provide solutions for current challenges in nanomedicine.

In cancer therapy, the administered cytostatics show a number of severe side-effects due to their toxicity.<sup>1,2</sup> Side effects can be reduced by encapsulating the drug in a delivery-system, which protects the body from the toxic drug and prevents the decomposition of the drug prior to reaching the target cells. Furthermore, a specific targeting of this drug carrier onto malign cells combined with a controlled release of the drug by diffusion minimizes the amount of drug that has to be administered. Clinically used nanocarriers for drugs consist, for example, of synthetic organic polymers<sup>3–5</sup> or liposomes,<sup>6</sup> yet especially cell-targeting and a controlled-release still represent a great challenge. Mesoporous silica materials, which contain nanometer-sized channel systems, provide high potential as novel drug-delivery systems due to their high versatility.<sup>7–12</sup> The physical properties that can be controlled include the surface properties, pore topologies, pore sizes, and surface areas.<sup>13,14</sup> These properties are essential for generating a depot-effect, that is, a retarded controlled release of a drug from the delivery system. They also provide flexibility for the incorporation of a high amount of differently sized guests. Additionally, silica nanostructures have a high potential for cell-targeting approaches as they can be covalently modified. Hence, mesoporous silica materials meet the essential requirements for a novel efficient class of drug-delivery systems.

In order to gain control over the release of the drug molecules from the delivery system, understanding the diffusion of the drug inside the porous hosts is of paramount importance. This process can be studied with various techniques such as pulsed-field gradient NMR,<sup>15</sup> neutron scattering<sup>16</sup> and fluorescence correlation spectroscopy (FCS).<sup>17,18</sup> Single-molecule fluorescence microscopy can additionally yield direct insights into mechanistic details of the host–guest interactions on a nanometer scale and allows the investigation of the characteristics of ensemble subpopulations separately. This technique can therefore open insights that are obscured by ensemble methods. We have recently used this technique to unravel the host–guest interplay in a large variety of periodic nanoporous silica materials.<sup>14,19–23</sup> Furthermore, we were able to control the guest dynamics through surface modifications.<sup>13</sup>

Here, we demonstrate the potential of surfactant-templated mesoporous silica materials<sup>24</sup> (Figure 1a) as delivery system for the anticancer drug Doxorubicin hydrochloride (Figure 1b). To our knowledge, this is the first time ever that a relevant drug has been characterized on a single molecule level. Doxorubicin and its analogues are widely used in chemotherapy, for example, for the treatment of Kaposi's sarcoma,<sup>25</sup> ovarian carcinoma,<sup>26</sup> or breast cancer.<sup>27</sup> However, Doxorubicin is also highly toxic especially to the heart and the kidneys, which limits its therapeutic applications. Novel drug-delivery strategies for that drug are thus urgently needed.

\* To whom correspondence should be addressed. E-mail: Christoph.Braeuchle@cup.uni-muenchen.de. Phone: +49-89-2180-77547. Fax: +49-89-2180-77548.

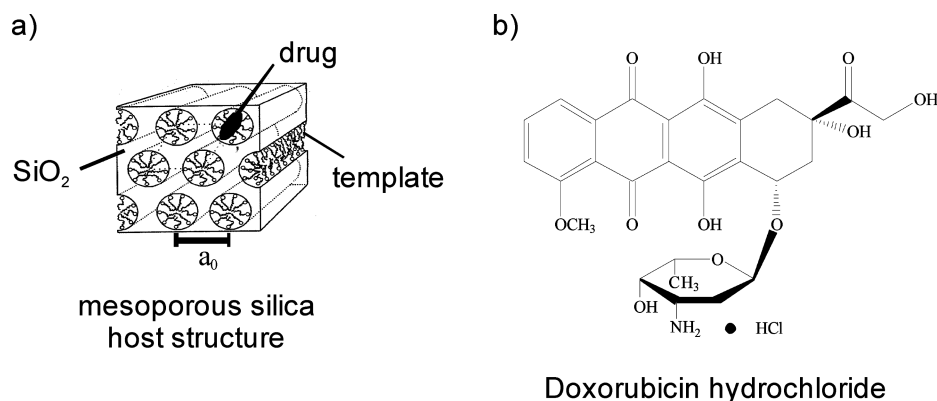


**Figure 1.** Host–guest-system. (a) Schematic of a surfactant-templated mesoporous silica material loaded with the cytostatic Doxorubicin hydrochloride.  $a_0$  designates the pore-to-pore distance. (b) Structure of the anticancer drug Doxorubicin hydrochloride.

Doxorubicin-loaded mesoporous samples were synthesized as thin films via the evaporation-induced self-assembly (EISA) method.<sup>28,29</sup> The following four mesoporous structures were synthesized and evaluated (see Supporting Information for details): (i) a cetyltrimethylammoniumbromide (CTAB)-templated film, (ii) a Pluronic P123-templated film, (iii) an unfunctionalized Brij-56-templated film, and (iv) a Brij-56-templated mesoporous film where the silica matrix has been functionalized with covalently attached propyl groups inside the porous network. Characterization via 1D X-ray diffractometry (XRD) (Table 1, Supporting Information) proved that all mesoporous thin films exhibit 2D-hexagonal order.<sup>14</sup> From the position of the diffraction peak ( $2\theta$ -value) the pore-to-pore distance  $a_0$  can be calculated. We thus determined  $a_0$  to be (i)  $4.4 \text{ nm} \pm 0.2 \text{ nm}$  for the CTAB-templated film, (ii)  $10 \text{ nm} \pm 0.5 \text{ nm}$  for the Pluronic P123-templated film, (iii)  $6.1 \text{ nm} \pm 0.3 \text{ nm}$  for the unfunctionalized Brij-56-templated film, and (iv)  $5.6 \text{ nm} \pm 0.3 \text{ nm}$  for the propyl-functionalized Brij-56-templated film. In the CTAB sample,  $a_0$  is significantly smaller than in the P123 sample due to the decreased size of the structure directing template. The Brij-56 samples show intermediate values. The propyl-functionalization leads to a decrease in  $a_0$  compared to the unfunctionalized film as observed previously.<sup>13</sup> A typical film thickness for the mesoporous structures investigated in this study is 150 nm.

We used single-molecule fluorescence microscopy to investigate the diffusion of Doxorubicin molecules inside the four mesoporous systems. In order to observe individual molecules, we incorporated Doxorubicin in highly diluted concentrations ( $10^{-10}$  to  $10^{-11}$  mol/L in the synthesis solution) into the mesoporous network. With a widefield fluorescence microscope, movies of the molecular motion inside the different samples were recorded (see Supporting Information for details of the setup). The position of the observable molecules was tracked by fitting a 2D Gaussian function<sup>30</sup> to the fluorescence signal throughout the movie, extracting molecular trajectories.<sup>20</sup> Since the film thickness lies far below the axial resolution of the microscope, the recorded molecular movement is always a two-dimensional projection of the real three-dimensional motion. Consequently, a 2D diffusion model is the correct model for data evaluation.

The Pluronic P123-templated samples were washed with water prior to the measurement in order to remove molecules on the film surface and thus prevent them from obscuring the measurement. In addition, the film surface was covered with PVA such that mobile molecules can only diffuse inside the channel system and not on the film surface. The recorded movies (see, e.g., Movie 1, Supporting Information) show two populations, 5% mobile and 95% immobile molecules. The presence of a majority of immobile molecules is surprising. In order to investigate this further, we recorded single molecule and ensemble fluorescence spectra of Doxorubicin (see Supporting Information). We detected two distinct populations of spectra in the films associated with the mobile and the immobile molecules. A concentration dependent characterization of the Doxorubicin fluorescence in solution (Supporting Information) allowed us to assign the immobile molecules in the films to Doxorubicin monomers and the diffusing population to Doxorubicin dimers. At low Doxorubicin concentrations, the monomer is the dominant species whereas an increase in concentration leads to a formation of dimers. During medical applications the delivery system will be loaded with high concentrations of Doxorubicin and the drug will be present mainly in the form of mobile aggregates. This mobility is an essential prerequisite for an efficient release from the delivery system. A trajectory of a mobile molecule, mapping the molecular motion through the channel network of the host silica structure, is given in Figure 2a. The drug molecules can diffuse throughout the porous network either along one pore or in a more restricted way from one pore to neighboring pores via defects, that is, openings in the channel walls. The trajectory appears not very well structured due to the small domain size inside these samples.

In contrast, highly structured trajectories were obtained for the mobile population in CTAB-templated mesoporous thin films. Figure 2b displays such a trajectory of a single Doxorubicin molecule, revealing the large linear domains inside these materials.<sup>19</sup> The domain size in the CTAB-templated samples is significantly larger than in the above-discussed P123-templated samples. Thus the trajectory is quite linear in contrast to the trajectory of Figure 2a. In the CTAB-templated samples, mobile and immobile molecules were found with a ratio of about 1:9 (see, e.g., Movie 2, Supporting Information).

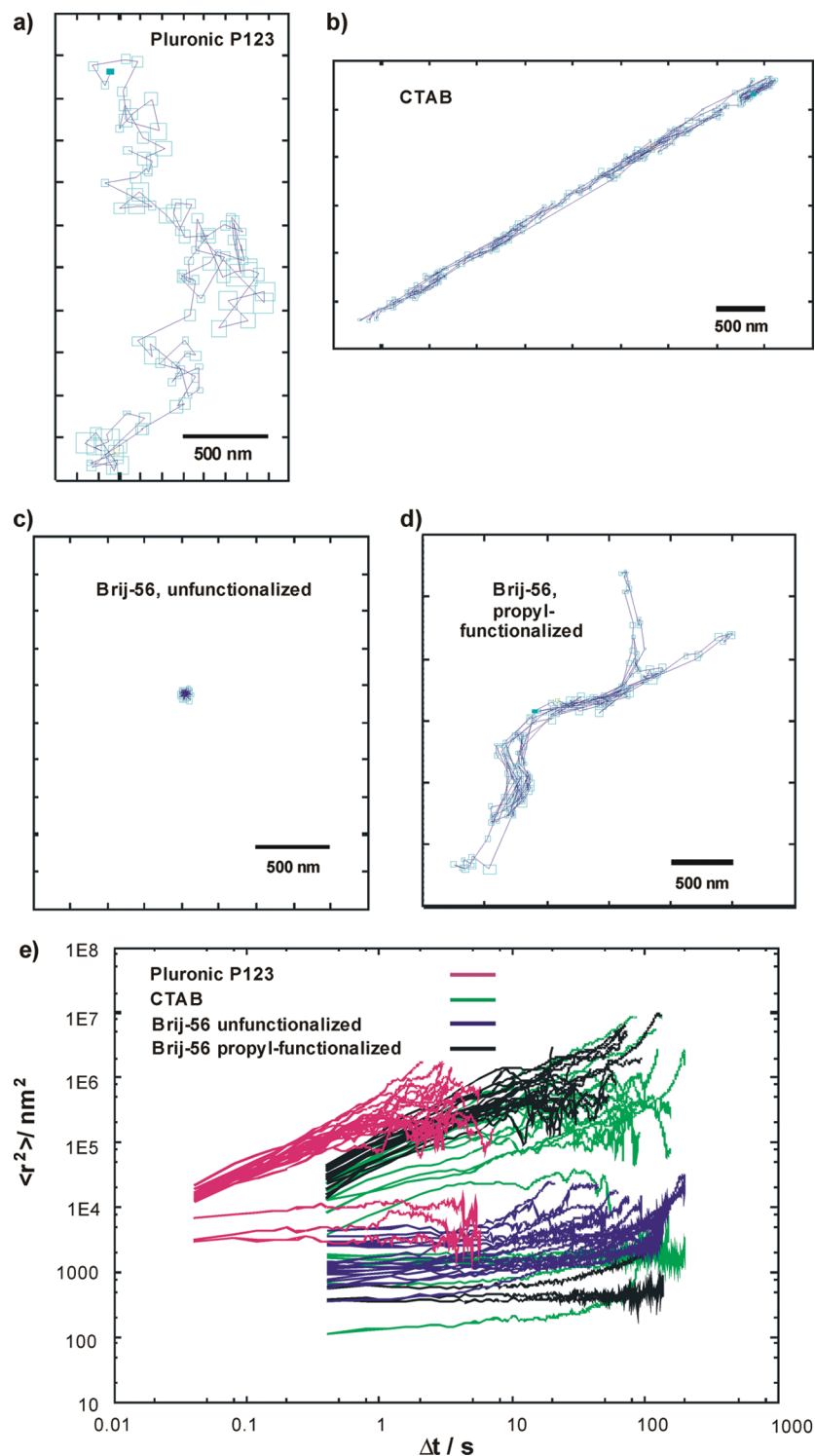


**Figure 2.** Single molecule diffusion of Doxorubicin in nanoporous systems. Exemplary trajectory of a molecule inside a (a) Pluronic P123, (b) CTAB, (c) unfunctionalized Brij-56, and (d) propyl-functionalized Brij-56-templated film. The small blue squares indicate the positioning accuracy for each point in the trajectory, which depends on the signal-to-noise ratio ( $\sim 60$  nm for P123,  $\sim 35$  nm for CTAB, and  $\sim 40$  nm for Brij-56-templated samples). While in panels a, b, and d the molecules are mobile, (c) depicts an immobile molecule appearing as a spot. (e) MSD as a function of time. Each line displays a MSD curve for a single Doxorubicin molecule. For the unfunctionalized Brij-56 sample (blue), only a single population of immobile molecules can be found. The CTAB (green), propyl-functionalized Brij-56 (black), and the Pluronic P123 samples (pink) show two distinguishable populations of mobile and immobile molecules. In each of the series, at least 20 molecules were evaluated. Only a selected number of MSD curves for immobile molecules has been plotted for clarity, thus the graph does not represent the real number ratio of molecules in the different populations.

Surprisingly, for the unfunctionalized Brij-56-templated thin films the evaluation of the recorded movies shows that all molecules were immobile (see, e.g., Movie 3 in the

Supporting Information). Figure 2c displays an exemplary single molecule “trajectory” of Doxorubicin inside an unfunctionalized Brij-56-templated film. The “trajectory” con-

sists of a blue spot, displaying the immobility of the molecule. We attribute the observed immobility to strong adsorption of the Doxorubicin to the hydroxyl groups in the channel walls. Recent work has shown that those hydroxyl groups can present adsorption sites.<sup>19,23</sup> They could interact via hydrogen bonding with the numerous oxygen atoms in the Doxorubicin molecule (see Figure 1b). In contrast, in the P123-templated samples the drug has more space to move since the pore-to-pore distance is increased by a factor of 1.6 compared to the unfunctionalized Brij-56 channel network. This apparently reduces the influence of the adsorption sites resulting in a mobile population. Interestingly, also in the CTAB-templated samples with a narrow pore-to-pore distance of 4.4 nm a mobile population of Doxorubicin was found. There are several effects that can contribute to the observed mobility in this system. The adsorption sites are shielded by the ionic template, which electrostatically saturates the channel surface and thus suppresses their capability of forming hydrogen bonds with the drug. Pluronic P123 and Brij-56 are nonionic templates that cannot effectively shield the hydroxyl groups. To test the hypothesis about the effects of ionic shielding, we performed additional experiments with varying sodium chloride ion concentrations inside the channel. We found that an increase in ion concentration leads to an increase in drug diffusivity (data not shown).

A mobile population can be recovered also for the Brij-56-templated samples by chemically modifying the walls with propyl functional groups. This leads to a hydrophobization of the pore inner surface through a shielding of the hydroxyl groups, resulting in weaker interactions between the drug and the host matrix. We recently found that propyl-functionalization increases the diffusivity of guest molecules inside mesoporous films compared to unfunctionalized films.<sup>13</sup> In the Brij-56-templated propyl-functionalized mesoporous film mobile and immobile molecules are observed with a ratio of  $\sim 1:9$  (see, e.g., Movie 3, Supporting Information). A single molecule trajectory of a mobile molecule is displayed in Figure 2d. The well-structured trajectory clearly maps the domain structure of the underlying porous network.<sup>14,22</sup>

In order to quantitatively compare the dynamics of the drug in the four different nanostructures the mean-square displacements (MSDs)  $\langle r^2(t) \rangle$  of the single Doxorubicin molecules were calculated (Figure 2e). The MSD results from the step lengths between the individual positions of the molecule in the above-discussed trajectories. In each of the series, at least 20 molecules were evaluated. Assuming a one-dimensional random walk ( $n = 1$ ) for CTAB-templated samples and a two-dimensional random walk ( $n = 2$ ) for Brij-56 and P123-templated samples, the MSD obeys

$$\langle r^2(t) \rangle = nDt \quad (1)$$

and therefore a diffusion coefficient  $D$  of the single molecule can be obtained.

For the CTAB-templated samples (green lines in Figure 2d), the two observed populations can be clearly distin-

guished: the immobile molecules show a constant MSD, as expected for a zero diffusion coefficient, whereas the diffusion dynamics of the mobile molecules is characterized by a MSD growing linearly with time. By averaging the single molecule diffusion coefficients, we compute the mean-diffusion coefficient for the entire mobile population as well as its standard deviation, giving  $\langle D_{\text{CTAB}} \rangle = 2.0 \times 10^4 \pm 2.3 \times 10^3 \text{ nm}^2/\text{s}$ . The determined deviation is caused by the inherent structural heterogeneity of the samples.

For the Pluronic P123-templated samples (pink lines in Figure 2d), the mean diffusion coefficient for the mobile population can be obtained as  $\langle D_{\text{P123}} \rangle = 5.4 \times 10^4 \pm 9.7 \times 10^3 \text{ nm}^2/\text{s}$ . This increase by a factor of 2.7 compared to the CTAB samples can be explained by the increased pore-to-pore distance (from 4.4 to 10 nm) and differences in the interactions between the drug and the different templates.

As expected, the MSDs for all molecules in the unfunctionalized Brij-56-templated films (blue lines in Figure 2d) are constant since the molecules are immobile.

For the mobile population in the propyl-functionalized Brij-56-templated samples (black lines), a mean diffusion coefficient  $\langle D_{\text{propyl-Brij}} \rangle = 1.6 \times 10^4 \pm 1.9 \times 10^3 \text{ nm}^2/\text{s}$  was determined, an  $\sim 3.4$ -fold reduction compared to the Pluronic-templated samples. This can be rationalized as the pore-to-pore distance is significantly smaller compared to P123-templated channels ( $a_0$  is reduced by a factor of  $\sim 2$ ), and the introduction of propyl groups inside the pore additional to the template further reduces the volume for the molecule to move.

This is the first time that a clinically relevant cytostatic has been monitored during its motion inside a nanoporous delivery system on a single molecule level. The data of Figure 2 clearly demonstrate the benefits of a single molecule approach to this study, as the different populations would have been obscured by the inevitable averaging associated with ensemble methods. We have shown that pore diameter control and pore functionalization offer possibilities to fine-tune host-guest interactions and are therefore also important techniques for controlling the dynamics of drug release. The existence of only 5–10% mobile molecules and up to 95% immobile molecules under single molecule conditions does not affect the efficiency of mesoporous silica as drug carriers. We demonstrate in Figure 5 (Supporting Information) that during medical applications, where Doxorubicin is present in high ensemble concentrations, the drug appears in the form of mobile dimers. Consequently, the drug will be efficiently released from the delivery system.

We tested this assumption using Doxorubicin-loaded Pluronic P123-templated mesoporous films (Doxorubicin concentration  $\sim 10^{-4} \text{ mol/L}$  in the synthesis solution) and determined the drug release kinetics in order to prove the applicability of the system. The P123-templated structures were chosen for this experiment because Pluronic is well known as biocompatible micellar nanocarrier for pharmaceuticals, such as Doxorubicin.<sup>4</sup> Figure 3a schematically represents the sample setup for the release and live-cell measurements. A coverslip with the Doxorubicin loaded mesoporous structure was mounted with a magnet inside the

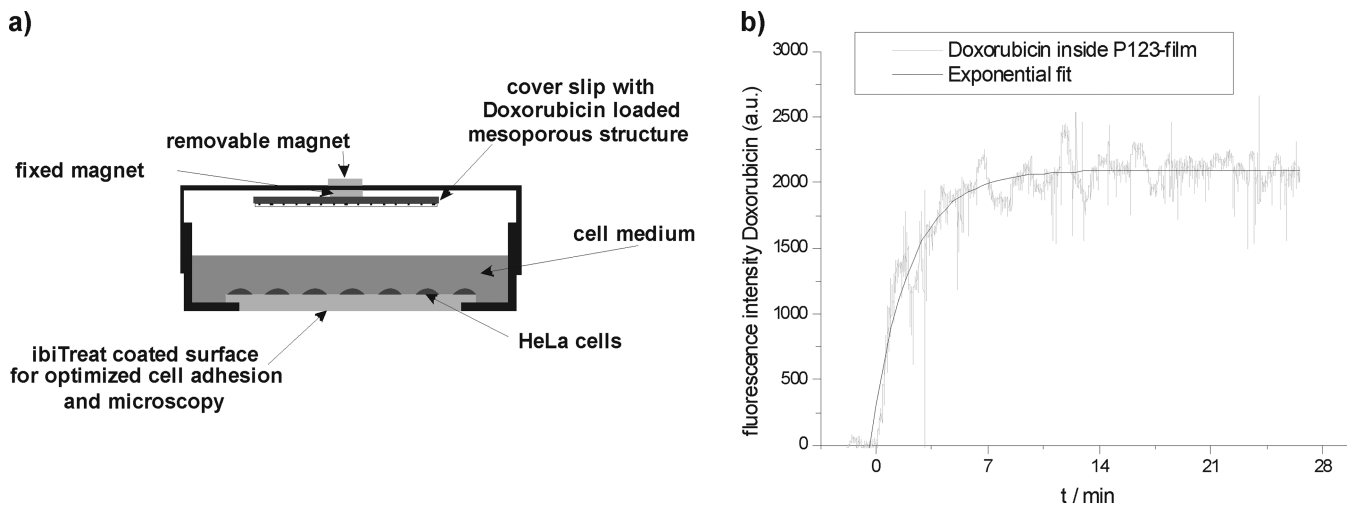


**Figure 3.** Drug release characterization. (a) Sample setup. The sample consists of a  $\mu$ -Dish with cell medium and HeLa cells adhered to the bottom of the dish. On the upper side of the dish, a coverslip with a Doxorubicin-loaded mesoporous structure is held using magnets. Upon removing the magnet, the sample is immersed into the cell medium, which can flush the pores of the delivery system and trigger the drug release. (b) Release kinetics of Doxorubicin from a Pluronic P123-templated thin film. The release was monitored via the rise of fluorescence intensity of Doxorubicin 50  $\mu\text{m}$  above the bottom of the  $\mu$ -Dish during time (gray curve). The black line shows an exponential fit to the data, according to eq 2.

top cover of a  $\mu$ -Dish directly above HeLa cells and cell medium (see Supporting Information for details). The mesoporous silica film was carefully rinsed with water before use in order to remove loosely bound Doxorubicin from the film surface, which otherwise could obscure the measurement. Upon removing the magnet on the upper side of the cover, the coverslip is immersed into the cell medium. The solution enters the pores and triggers the Doxorubicin release from the mesoporous system. The increase in fluorescence intensity of Doxorubicin in the cell medium 50  $\mu\text{m}$  above the bottom of the  $\mu$ -Dish was monitored with a confocal microscope (Supporting Information). During the measurement, the sample was stirred to guarantee a homogeneous distribution of the Doxorubicin molecules released into solution. Control experiments (Supporting Information) show that this increase in intensity is caused by the release of Doxorubicin from the porous network in the film and is not simply due to Doxorubicin detaching from the film surface.

Figure 3b shows the increase of Doxorubicin fluorescence intensity (gray curve). Within the first few minutes after adding the drug loaded coverslip to the cell medium, no Doxorubicin fluorescence could be detected. We interpret this as the time the cell medium needs to flush the pores and trigger the drug release. Once the release has started ( $t = 0$ ), the Doxorubicin fluorescence rapidly increases. The data were fitted to the following exponential equation

$$y = A \times \left(1 - \exp - \left(\frac{x}{t_r}\right)\right) \quad (2)$$

where the amplitude  $A$  corresponds to the maximum fluorescence intensity and  $t_r$  is the characteristic release time. The good agreement between fit and experimental data shows that the release follows a first-order kinetics. By averaging the release times from the experiments, we obtain a mean release-time  $\langle t_r \rangle = 3.2 \text{ min} \pm 0.8 \text{ min}$ . After about 10 min,

most of the drug has been released. Thus, a drug incorporated in the delivery system can efficiently be delivered to the surrounding solution. After the release, the thin film was still intact according to X-ray data (data not shown). Cauda et al. found a similar release kinetics for the antibiotic Vancomycin from mesoporous silica.<sup>31</sup> For an unfunctionalized Brij-56-templated film, where all molecules are immobile (see Figure 2e), no significant increase in Doxorubicin fluorescence and thus no drug release can be detected in the cell medium (see Figure 6 in the Supporting Information). Therefore, the diffusion dynamics within the film directly affects the release kinetics from the film.

While these studies present a major breakthrough for the application of mesoporous materials as drug carriers, for therapeutic applications mesoporous structures can also be capped in order to prevent an early release of the drug from the delivery system prior to reaching the target-site. Different strategies for capping the pores were recently developed. Schlossbauer et al. have introduced biotin-avidin as enzyme-responsive cap system for mesoporous silica.<sup>32</sup> This cap system opens through protease-triggered hydrolysis of the avidin. Furthermore, CdS nanocrystals have been used as caps on mesoporous silica, for example, for the controlled release of neurotransmitters.<sup>10</sup> In this case, cap opening is stimulated by reducing agents. In a further approach by Giri et al., magnetic nanoparticles have been employed to cap mesoporous silica nanostructures.<sup>12</sup> Thus, combining the drug-loaded mesoporous structures with one of the above-discussed capping approaches can add a further functionality to these drug-delivery systems.

Next, we investigated the effect of the delivered Doxorubicin onto HeLa cells. Figure 4 shows overlays of confocal transmission images (gray) and fluorescence images of the Doxorubicin fluorescence (red). According to their shape, the HeLa cells were alive before being exposed to Doxorubicin (Figure 4a). The transmission image shows the adhered

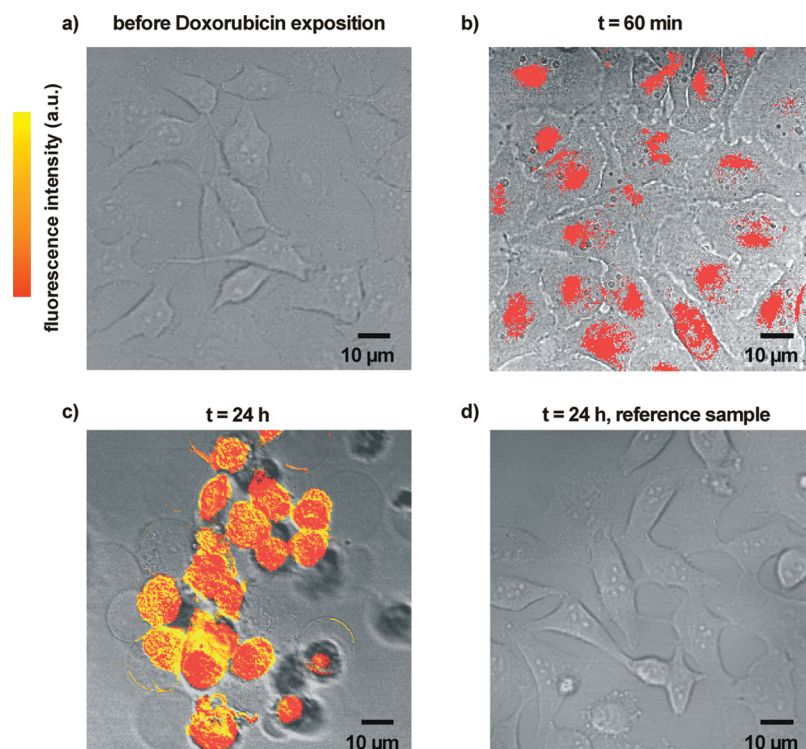


**Figure 4.** Live-cell measurements. Overlay of confocal transmission images (gray) and Doxorubicin fluorescence (red). Images (a) before, (b) 60 min, and (c) 24 h after adding the Doxorubicin-loaded delivery system are shown. (d) Image recorded 24 h after adding an unloaded delivery system as reference.

cells on the bottom of the  $\mu$ -Dish. No Doxorubicin fluorescence was detected at this stage of the experiment. After  $t = 60$  min, Doxorubicin fluorescence could clearly be located inside the cell nucleus (Figure 4b). This can be rationalized as the cytostatic properties of Doxorubicin mainly arise from direct intercalation into DNA as well as inhibition of topoisomerase II by interfering with the topoisomerase II-DNA complex.<sup>33</sup> However, the cells still appeared to be alive according to the underlying transmission image. After  $t = 24$  h, the cells were highly fluorescing (Figure 4c), showed a round shape, and had detached from the bottom of the  $\mu$ -Dish, indicating cell death. These effects were caused by the drug itself, as demonstrated by control experiments with a Doxorubicin-free delivery system (Figure 4d). This proves that Doxorubicin released from thin films is still cytostatic and the mesoporous films can thus be applied for drug-delivery purposes.

In conclusion, we have shown that mesoporous thin films with nanometer-sized pores can be used as drug-delivery system for the cytostatic Doxorubicin. Our single molecule approach offers detailed mechanistic insights into the complicated host-guest interplay. We have demonstrated how the interaction of the drug with the host-matrix can be influenced on a nanometer-scale via covalently attached organic functional groups. Such fine-tuning of the host-guest interaction is an essential prerequisite for generating a depot-effect. Furthermore, we have shown that the drug can be released from the nanochannels in the carrier system and can be taken up by cells. For future applications mesoporous structures could be used either in the form of nanoparticles for drug-delivery applications, for example in cancer therapy,

or in the form of film coatings for implants, for example, for the delivery of immunosuppressive drugs to diminish rejection. Hence, a wide range of different drugs is within the scope for this novel class of delivery systems.

**Acknowledgment.** We are very thankful to T. Bein from the Department of Chemistry and Biochemistry, University of Munich for helpful discussions. We thank G. Winter and S. Tinkov from the Department of Pharmacy, University of Munich for providing us laboratory equipment for the safe preparation and handling of the cytostatic samples as well as for helpful introductions into the chemistry of Doxorubicin. Further, we thank E. Wagner from the Department of Chemistry and Biochemistry, University of Munich, for fruitful discussions. Financial support from the Nanosystems Initiative Munich (NIM) and the SFBs 486 and 749 (all DFG) is gratefully acknowledged.

**Supporting Information Available:** Synthesis recipes, experimental methods, widefield movies, and control experiments. This material is available free of charge via the Internet at <http://pubs.acs.org>.

## References

- (1) Guchelaar, H. J.; Ten Napel, C. H. H.; De Vries, E. G. E.; Mulder, N. H. *Clin. Oncol.* **1994**, *6*, 40–48.
- (2) Mann, D. L. *Nat. Med.* **2006**, *12* (8), 881–882.
- (3) Langer, R. *Science* **1990**, *249* (4976), 1527–1533.
- (4) Torchilin, V. P. *Pharm. Res.* **2007**, *24* (1), 1–16.
- (5) Uhrich, K. E.; Cannizzaro, S. M.; Langer, R. S.; Shakesheff, K. M. *Chem. Rev.* **1999**, *99*, 3181–3198.
- (6) Samad, A.; Sultana, Y.; Aqil, M. *Curr. Drug Delivery* **2007**, *4* (4), 297–305.
- (7) Slowing, I. I.; Trewyn, B. G.; Giri, S.; Lin, V. S. Y. *Adv. Funct. Mater.* **2007**, *17* (8), 1225–1236.

- (8) Lu, J.; Liong, M.; Zink, J. I.; Tamanoi, F. *Small* **2007**, *3* (8), 1341–1346.
- (9) Prokopowicz, M.; Przyjazny, A. *J. Microencapsulation* **2007**, *24* (7), 694–713.
- (10) Lai, C.-Y.; Trewyn, B. G.; Jęftinija, D. M.; Jęftinija, K.; Xu, S.; Jęftinija, S.; Lin, V. S. Y. *J. Am. Chem. Soc.* **2003**, *125*, 4451–4459.
- (11) Roy, I.; Ohulchansky, T. Y.; Bharali, D. J.; Pudavar, H. E.; Mistretta, R. A.; Kaur, N.; Prasad, P. N. *Proc. Natl. Acad. Sci. U.S.A.* **2005**, *102* (2), 279–284.
- (12) Giri, S.; Trewyn, B. G.; Stellmaker, M. P.; Lin, V. S. Y. *Angew. Chem., Int. Ed.* **2005**, *44* (32), 5038–5044.
- (13) Lebold, T.; Mühlstein, L. A.; Blechinger, J.; Riederer, M.; Amenitsch, H.; Köhn, R.; Peneva, K.; Müllen, K.; Michaelis, J.; Bräuchle, C.; Bein, T. *Chem.—Eur. J.* **2009**, *15* (7), 1661–1672.
- (14) Kirstein, J.; Platschek, B.; Jung, C.; Brown, R.; Bein, T.; Bräuchle, C. *Nat. Mater.* **2007**, *6* (4), 303–310.
- (15) Kukla, V.; Kornatowski, J.; Demuth, D.; Girnus, I.; Pfeifer, H.; Rees, L. V. C.; Schunk, S.; Unger, K. K.; Kärger, J. *Science* **1996**, *272* (5262), 702–704.
- (16) Benes, N. E.; Jobic, H.; Verweij, H. *Microporous Mesoporous Mater.* **2001**, *43* (2), 147–152.
- (17) Fu, Y.; Ye, F. M.; Sanders, W. G.; Collinson, M. M.; Higgins, D. A. *J. Phys. Chem. B* **2006**, *110* (18), 9164–9170.
- (18) Wirth, M. J.; Swinton, D. J.; Ludes, M. D. *J. Phys. Chem. B* **2003**, *107*, 6258–6268.
- (19) Jung, C.; Kirstein, J.; Platschek, B.; Bein, T.; Budde, M.; Frank, I.; Müllen, K.; Michaelis, J.; Bräuchle, C. *J. Am. Chem. Soc.* **2008**, *130* (5), 1638–1648.
- (20) Hellriegel, C.; Kirstein, J.; Bräuchle, C. *New J. Phys.* **2005**, *7*, 23–36.
- (21) Jung, C.; Hellriegel, C.; Michaelis, J.; Bräuchle, C. *Adv. Mater.* **2007**, *19* (7), 956–960.
- (22) Zürner, A.; Kirstein, J.; Dobliger, M.; Bräuchle, C.; Bein, T. *Nature* **2007**, *450* (7170), 705–709.
- (23) Jung, C.; Hellriegel, C.; Platschek, B.; Wohrle, D.; Bein, T.; Michaelis, J.; Bräuchle, C. *J. Am. Chem. Soc.* **2007**, *129* (17), 5570–5579.
- (24) Beck, J. S.; Vartuli, J. C.; Roth, W. J.; Leonowicz, M. E.; Kresge, C. T.; Schmitt, K. D.; Chu, C. T. W.; Olson, D. H.; Sheppard, E. W.; McCullen, S. B.; Higgins, J. B.; Schlenker, J. L. *J. Am. Chem. Soc.* **1992**, *114* (27), 10834–10843.
- (25) Wagner, D.; Kern, W. V.; Kern, P. *Clin. Invest.* **1994**, *72* (6), 417–423.
- (26) Collins, Y.; Lele, S. *J. Nat. Med. Assoc.* **2005**, *97*, 1414–1416.
- (27) O’Shaughnessy, J. *Oncologist* **2003**, *8*, 1–2.
- (28) Brinker, C. J.; Lu, Y. F.; Sellinger, A.; Fan, H. Y. *Adv. Mater.* **1999**, *11* (7), 579–585.
- (29) Please note: Doxorubicin may cause cancer. Especially during the spin-coating process harmful aerosols are generated. Working under especially equipped safety benches is mandatory. Respiratory protection and other equipment to avoid exposure are necessary.
- (30) Schmidt, T.; Schuetz, G. J.; Baumgartner, W.; Gruber, H. J.; Schindler, H. *J. Phys. Chem.* **1995**, *99* (49), 17662–17668.
- (31) Cauda, V.; Onida, B.; Platschek, B.; Mühlstein, L.; Bein, T. *J. Mater. Chem.* **2008**, *18* (48), 5888–5899.
- (32) Schlossbauer, A.; Kecht, J.; Bein, T. *Angew. Chem., Int. Ed.* **2009**, *48*, 3092–3095.
- (33) D’Arpa, P.; Liu, L. F. *Biochim. Biophys. Acta* **1989**, *989* (2), 163–177.

NL9011112